Report No. 65

On-Axis Polarization Coupling in y-Cut Titanium In-Diffused Lithium Niobate Slab Waveguides

Stephen L. Kwiatkowski, Alan R. Mickelson,
and Dag R. Hjelme

November 1994

Guided Wave Optics Laboratory
Department of Electrical and Computer Engineering
University of Colorado at Boulder
Boulder, Colorado 80309-0425

unclassified
SECURITY CLASSIFICATION OF THIS PAGE

REPORT DOCUMENTATION PAGE

Form Approved OMB No. 0704-0188

1a. REPORT SECURITY CLASSIFICATION: unclassified	1b. RESTRICTIVE MARKINGS: none
2a. SECURITY CLASSIFICATION AUTHORITY: DISCASS	3. DISTRIBUTION/AVAILABILITY OF REPORT: unrestricted
2b. DECLASSIFICATION/DOWNGRADING SCHEDULE: N/A	
4. PERFORMING ORGANIZATION REPORT NUMBER(S): ECE/GWOL/ 65	5. MONITORING ORGANIZATION REPORT NUMBER(S): DOD-ONRN00014-92-J-1190
6a. NAME OF PERFORMING ORGANIZATION: University of Colorado; 6b. OFFICE SYMBOL (If applicable):	7a. NAME OF MONITORING ORGANIZATION: Office of Naval Research, Attn: Dr. Arthur Jordan, Code 1114 SE
6c. ADDRESS (City, State, and ZIP Code): Electrical & Computer Engineering Dept., Boulder, CO 80309-0425	7b. ADDRESS (City, State, and ZIP Code): 800 N. Quincy Avenue, Arlington, VA, 22217-5000
8a. NAME OF FUNDING/SPONSORING ORGANIZATION: Office of Naval Research; 8b. OFFICE SYMBOL (If applicable):	9. PROCUREMENT INSTRUMENT IDENTIFICATION NUMBER
8c. ADDRESS (City, State, and ZIP Code): 800 N. Quincy Avenue, Arlington, VA 22217-5000	10. SOURCE OF FUNDING NUMBERS: PROGRAM ELEMENT NO. / PROJECT NO. / TASK NO. / WORK UNIT ACCESSION NO.

11. TITLE (Include Security Classification)
(u) On-Axis Polarization Coupling in y-Cut Titanium In-Diffused Lithium Niobate Slab Waveguides

12. PERSONAL AUTHOR(S)
S. L. Kwiatkowski, A. R. Mickelson, and D. R. Hjelme

13a. TYPE OF REPORT	13b. TIME COVERED	14. DATE OF REPORT (Year, Month, Day)	15. PAGE COUNT
technical	FROM ____ TO ____	October 1994	40

16. SUPPLEMENTARY NOTATION

17. COSATI CODES			18. SUBJECT TERMS (Continue on reverse if necessary and identify by block number)
FIELD	GROUP	SUB-GROUP	

19. ABSTRACT (Continue on reverse if necessary and identify by block number)

We report on polarization coupling from x-propagating TE-polarized waveguide modes to TM-polarized radiation modes in y-cut titanium in-diffused lithium niobate slab waveguides. The polarization coupling is linear with respect to the TE-polarized input power and depends on the titanium diffusion time. Furthermore, the polarization coupling was not affected by white light flooding the waveguide. The maximum conversion from a TE-polarized waveguide mode to a TM-polarized radiation mode is 3.2%/cm using a conservative estimate for the power initially in the TE waveguide mode. We observe no turn-on delay greater than 1 s between the excitation of the TE waveguide mode and the observation of the TM radiation. In addition, intentional amplitude modulations of the TE-polarized waveguide mode were registered as equivalent amplitude modulations by the TM-polarized radiation modes. We did not observe polarization coupling from x-propagating TM-polarized waveguide modes to TE-polarized radiation modes.

20. DISTRIBUTION/AVAILABILITY OF ABSTRACT: ☑ UNCLASSIFIED/UNLIMITED ☐ SAME AS RPT. ☐ DTIC USERS	21. ABSTRACT SECURITY CLASSIFICATION: unclassified
22a. NAME OF RESPONSIBLE INDIVIDUAL: Alan R. Mickelson	22b. TELEPHONE (Include Area Code): 303/492-7539; 22c. OFFICE SYMBOL:

DD Form 1473, JUN 86 Previous editions are obsolete. SECURITY CLASSIFICATION OF THIS PAGE

On-axis polarization coupling in y-cut titanium in-diffused lithium niobate slab waveguides

Stephen L. Kwiatkowski and Alan R. Mickelson

Department of Electrical and Computer Engineering

University of Colorado at Boulder

Boulder, Colorado 80309

Dag. R. Hjelme

SINTEF-DELAB

Norwegian Institute of Technology

N-74034

Trondheim, Norway

Abstract

We report on polarization coupling from x-propagating TE-polarized waveguide modes to TM-polarized radiation modes in y-cut titanium in-diffused lithium niobate slab waveguides. The polarization coupling is linear with respect to the TE-polarized input power and depends on the titanium diffusion time. Furthermore, the polarization coupling was not affected by white light flooding the waveguide. The maximum conversion from a TE-polarized waveguide mode to a TM-polarized radiation mode is 3.2 %/cm using a conservative estimate for the power initially in the TE waveguide mode. We observe no turn-on delay greater than 1 s between the excitation of the TE

waveguide mode and the observation of the TM radiation. In addition, intentional amplitude modulations of the TE-polarized waveguide mode were registered as equivalent amplitude modulations by the TM-polarized radiation modes. We did not observe polarization coupling from x-propagating TM-polarized waveguide modes to TE-polarized radiation modes. This polarization coupling is a source of loss and potentially a source of noise for titanium in-diffused lithium niobate optical devices.

Keywords: lithium niobate, titanium in-diffusion, polarization coupling, optical waveguide.

I. INTRODUCTION

This work describes polarization coupling in titanium in-diffused lithium niobate slab waveguides: a source of polarization dependent loss and potentially a source of noise, in integrated-optical devices.

We are developing a methodology for the fabrication and testing of titanium in-diffused lithium niobate (Ti:$LiNbO_3$) [1] slab waveguides. One unexpected result of this work has been the observation of polarization coupling in these slab waveguides. When we couple transverse electric field (TE) polarized light into waveguide modes, we observe transverse magnetic field (TM) radiation modes radiating from the waveguide. Since this polarization coupling occurs for propagation along the crystal axis, the observed TM radiation can be distinguished from the TM radiation that would result from leaky modes propagating off-axis in an anisotropic waveguide. When the polarization of the input was changed to TM-polarized, we did not observe polarization coupling into TE-polarized radiation

modes.

There are previous reports of polarization coupling in y-cut Ti:$LiNbO_3$ for on-axis propagation of TE waveguide modes. However, the properties of the TM radiation and the circumstances yielding the polarization coupling in these reports are different from those in our experiments. For example, Kazansky [2] reports a nonlinear coupling between TE and TM modes in x-propagating y-cut Ti:$LiNbO_3$ channel waveguides. One of his results shows a nonlinear relationship between the power of the input TE light and the power of the TM radiation. Another measurement shows a delay of the order of tens of minutes between the input of the TE light and the onset of the TM radiation. Kazansky proposes that the mechanism for the polarization coupling is a grating caused by the nonlinear circular photovoltaic effect and directed perpendicular to the plane of the waveguide. This grating couples TE waveguide modes into TM radiation modes. Since we found neither the power nonlinearity nor the delay of onset, our observations are probably not the result of the same mechanism suggested by Kazansky.

Other observations of polarization coupling from TE waveguide modes to TM radiation modes in lithium niobate waveguides are those reported by Chen and Chang [3]. They report an anomalously large attenuation loss for x-propagating TE waveguide modes in waveguides formed by proton-exchange in y-cut lithium niobate. This attenuation was observed for TE modes whose effective index is less than the substrate's ordinary index. Furthermore, this attenuation is associated with polarization coupling into TM radiation modes. The TE waveguide modes with an effective index greater than the substrate's ordinary index experience neither polarization coupling nor increased propagation loss. Chen and Chang do not mention either a nonlinear power relationship between the TE or TM modes nor an onset delay between the TE-polarized and TM-polarized modes.

The polarization coupling seen by Chen and Chang has a similar characteristic to the polarization coupling we see. We both observe polarization coupling from TE guided modes whose effective index is less than the TM substrate's index of refraction. Our observations come from waveguides formed by titanium in-diffusion, not proton exchange. In their search for the mechanism causing this phase-matched polarization coupling, Chen and Chang ruled out scattering from surface defects, but otherwise stated that the mechanism is not well understood.

Another situation which yields TM-polarized light radiating from a predominantly TE-polarized waveguide mode is when modes propagate off-axis in anisotropic waveguides. Theoretical studies of these leaky modes in anisotropic slab waveguides has been extensively reported in the literature; see for example [4–11]. Experimental verification of leaky modes in uniaxial waveguides have been reported for y-cut Ti:$LiNbO_3$ [12,13]. We also have observed leaky modes, but in lithium out-diffused y-cut $LiNbO_3$ slab waveguides. For propagation directions not along a crystal axis, these leaky modes exist with a hybrid polarization containing all six field components. For the specialized waveguide orientations which yield on-axis mode propagation, no leaky modes result, and these modes are characterized as uncoupled TE- and TM-guided modes.

This paper presents our measurements of TE to TM polarization coupling for propagation along the crystal's x-axis in y-cut Ti:$LiNbO_3$ slab waveguides. Our observations differ from [2] in that we do not measure a nonlinear relationship between the power of the TM radiation and the power of the TE waveguide mode, nor do we observe a delay between the input time of the TE waveguide mode and the onset of the TM radiation. Furthermore, the polarization coupling that we observe occurs for mode propagation along the crystal axis and thus cannot be explained only by leaky mode theory, which describes off-axis mode propagation

in anisotropic waveguides.

The outline of this paper is as follows. In the second section we describe our waveguide fabrication procedures. The third section contains the description of our experimental technique, and the fourth section presents the results of our measurements and observations. In the fifth and final section, we compare and contrast our results with other published observations of coupling between orthogonal polarizations and discuss the possible mechanisms which cause this polarization coupling.

II. WAVEGUIDE FABRICATION

The slab waveguides discussed in this paper were fabricated on the minus face of optical grade y-cut lithium niobate wafers [14]. The orientation of the slab waveguide with respect to the substrate's crystal axes is shown in Fig. 1. The propagation of the guided modes is predominantly along the crystal's x-axis. Typical dimensions for the rectangular waveguide specimens are 1 cm to 3 cm along the x-axis, 0.1 cm along the y-axis, and 1 cm along the z-axis.

According to the manufacturer, these lithium niobate wafers originate from a crystalline boule that is grown using the Czochralski technique. The crystalline boule is drawn from a congruent melt of high purity Nb_2O_5 and $LiCO_3$ powders (less than 2 ppm of each transition metal, including iron). The congruent composition value of the melt is 48.38 $\pm$0.015 mole-% Li_2O. The resulting crystalline boule has compositional uniformity less than $\pm$0.005 mole-% Li_2O.

We fabricated two different types of slab waveguides on the LiNbO3 substrates. One type of waveguide was formed using titanium in-diffusion [1]. The fabrication procedure for these waveguides is as follows. Titanium metal was evaporated onto

an entire wafer in order to insure uniformity of the titanium thickness for each waveguide specimen. The titanium metal was evaporated by resistive heating in a vacuum of 5×10^{-4} Pa to a thickness of 25 nm as determined by a quartz crystal oscillator. Individual specimens were cut from this metalized wafer and then placed in a high temperature oven for the desired diffusion time.

The temperature schedule for the diffusion begins at room temperature and reaches the diffusion temperature, T=1000 °C , after a 2 h ramp-up time. The diffusion temperature is maintained for a time t. Afterwards, the specimens cooled to room temperature within two hours. The diffusion was carried out in an atmosphere of wet oxygen which was created by bubbling medical grade oxygen through a 17 cm column of room-temperature de-ionized water. This wet oxygen flowed at a rate of 300 l/h, into the oven chamber. We began flowing the wet oxygen during the temperature ramp-up at 345 ± 50 °C , and the wet oxygen continued to flow until the ramp-down temperature of 140 ± 25 °C . The final step consisted of polishing the specimen endfaces to optical quality use in input and output optical coupling. Specimen 41 was fabricated with a dwell time of 1 h while specimen 42 has a 2 h dwell time.

The second type of waveguide was fabricated without the titanium metalization. Our intention was to form lithium out-diffused waveguides [15,16]. However, subsequent studies [17] indicate that waveguide formation in these specimens may involve other processes in addition to lithium out-diffusion.

Waveguides of the second type were fabricated in the same manner as the titanium in-diffused waveguides but with the following differences: the waveguide originated from a different yet similar $LiNbO_3$ wafer, and the polishing of the specimen endfaces preceded the out-diffusion step. Specimen 53 is a waveguide of the second type with a 2 h dwell time.

III. WAVEGUIDE CHARACTERIZATION

The effective index N_{eff} of a waveguide mode is measured using prism out-coupling [18]. Light from a HeNe laser at wavelength $\lambda = 0.6328\,\mu$m is butt-coupled into the slab waveguide using a single-mode polarization-maintaining fiber. The extinction ratio between the two orthogonally polarized modes of the fiber was greater than 400:1. A rutile prism with its optic axis parallel to the substrate's optic axis is pressed against the waveguide to couple light out from the waveguide. At the output face of the prism the out-coupled light, or m-line, is refracted into air at the mode angle θ'_m. The mode's effective index is related to the mode angle by [19]

$$N_{eff} = n_p \sin\left[\theta_p + \arcsin\left(\frac{n_c}{n_p}\sin\left(\theta'_m\right)\right)\right], \tag{1}$$

where $n_p = 2.8666$ [20] is the prism's extraordinary index, $\theta_p = 60.59 \pm 0.02°$ is the prism's angle, and $n_c = 1.0003$ is the index of air.

We determine the mode angle θ'_m using two aligned translation stages, one with travel parallel to the prism output face and one with travel perpendicular to the prism output face. A charge-coupled device (ccd) array is affixed to these stages at a distance of 1 m from the prism output face. The m-line illuminates the ccd array, and a profile of the m-line is viewed on a digital oscilloscope. The angle θ'_m is determined using inverse triangulation. A right triangle is formed by translating the ccd array a distance Δx and a perpendicular distance Δy. For a particular stage translation Δx, the translation Δy is determined by repositioning the m-line at the location on the ccd array. Now, the mode angle can be calculated using the equation

$$\tan\left(\theta'_m\right) = \frac{\Delta x}{\Delta y}\,. \tag{2}$$

In a similar manner, we determine the substrate effective index N_s by measuring mode angle associated with the substrate m-line. Then we calculate the increment $\Delta N_{eff} = N_{eff} - N_s$ by which the effective index of the mode exceeds the substrate index. Using this technique, we eliminate the influences of systematic measurement errors at the expense of reporting relative, rather than absolute values for the effective index. Details of the measurement can be found in Ref. [17].

The experimental arrangement used for observing TM radiation is shown in Fig. 2. The same fiber-coupled light source used for the m-line measurements is used here to butt-couple into the waveguide. The maximum power output from the fiber is 230 μW. A polarizer and viewing screen are positioned far enough from the waveguide output face that the polarization content of the radiation pattern can be investigated. The fiber source is oriented so that TE polarized light is coupled into a set of slab waveguide modes which will propagate in the plane of the waveguide with an angular extent $\pm\theta_b$ about the x-axis. This maximum divergence angle θ_b was calculated by fitting a Gaussian profile to the fiber mode field and using the properties of Gaussian beam propagation in an isotropic and homogeneous medium [21]. The propagation angle is calculated from the equation

$$\theta_b = \arctan\left(\frac{\lambda}{\pi\omega_0 N_{eff}}\right), \tag{3}$$

where ω_0 is the beam radius where the intensity is reduced from the peak value by a factor of e^{-2}. Using the values $\omega_0 = 1.5\mu$mfrom a near-field measurement, $\lambda =$ 0.6328 μm, and $N_{eff} = 2.22$, we calculate that the waveguide modes propagate within the angular range of $\pm\theta_b = 3.5°$ to the crystal's x-axis.

Any TM radiation modes which are phase-matched to the TE waveguide modes will propagate at the phase-matching angle $\pm\phi$ with respect to the plane of the

waveguide; see Fig. 3. The phase-matching condition is given by

$$\cos(\phi) = \frac{N_{eff}}{n_o}, \tag{4}$$

where N_{eff} is the effective mode index and n_o is the substrate's ordinary index. This TM radiation undergoes total internal reflection at both air-$LiNbO_3$ interfaces and then emerges from the specimen at the waveguide endface in two branches, labeled A and B. These two branches of TM radiation emerge the sample with angles $\pm\phi'$ which are related to the phase matching angle ϕ through Snell's law,

$$\sin(\phi') = n_o \sin(\phi). \tag{5}$$

A two-dimensional ccd array was positioned in the path of branch A to record the detailed structure of the TM radiation pattern. The angular extent of the TM radiation pattern captured by the ccd array corresponds to a propagation angle of $\theta = \pm 3°$ about the crystal's x-axis.

We quantified the polarization coupling by measuring the power ratio ρ per unit propagation length of TM-polarized radiation to the TE-polarized input. To determine the value of ρ, a cylindrical lens, a power meter, and a polarizer were positioned at the output face of the waveguide so as to measure the TM radiation power in branch A. The TE input power to the waveguide was determined by measuring the output power of the fiber with the same power meter and polarizer combination. The measured TE input power should be multiplied by a factor of 2 to account for the loss in the polarizer in order to estimate the TE input power present at the waveguide.

Since only one branch of the TM radiation was collected by the power meter, the measured value of the TM power was multiplied by a compensating factor

Γ to obtain the total TM power. The compensation factor is determined by calculating the relative powers expected in each TM radiation branch. In general, the TM power in each branch will not be equal; see Fig. 3. The relative power in each branch depends on the geometrical properties of the particular sample, for example, the length of the waveguide and the thickness of the substrate. As Fig. 3 shows, more of the waveguide length contributes to the TM radiation in branch B than to branch A. For the case illustrated in Fig. 3, the total TM power radiated by the waveguide would be equal to the power measured in branch A multiplied by the compensation factor $\Gamma = 3$. The calculated values of ρ using this method will underestimate the amount of polarization coupling because (1) the calculation assumes complete power transfer from the input fiber to the TE waveguide modes and (2) the calculation excludes the possibility of TM radiation coupling back into the TE waveguide mode.

The degree of linearity between the TM radiation power and the input TE power was measured using the same experimental setup as that used for determining ρ. The power linearity was measured by varying the input TE power while measuring the TM power in branch A. The TE input power was varied by adjusting the laser power coupled into the polarization maintaining fiber.

We illuminate the specimen with a 250 W quartz halogen lamp to test for the presence of a photorefractive grating within the waveguide. An optical fiber bundle delivers the whitelight to the waveguide.

IV. EXPERIMENTAL RESULTS

Measured values of ΔN_{eff} are shown in Table I for the TE modes in the titanium in-diffused waveguide specimens 41 and 42, and for the TE modes in

the plain $LiNbO_3$ specimen, 53. Specimens 41 and 42 also supported TM-guided modes, whereas we did not observe any TM waveguide modes in specimen 53. The values of ΔN_{eff} were determined from regions of the m-lines that correspond to the propagation direction of the waveguide mode along the crystal's x-axis. Also listed in Table I are the calculated phase-matching angles ϕ for each mode.

Figure 4 displays the titanium concentration of specimen 42 after diffusion. Titanium concentration was measured using secondary ion mass spectroscopy (SIMS) [22]. The evaporated titanium layer appears to be fully diffused into the $LiNbO_3$ substrate with no residual surface titanium layer. The measurements of titanium concentration agree well with the Gaussian solution to the diffusion equation with source layer thickness much less than the diffusion depth [23].

The intensity radiation pattern for each specimen was studied using the experimental setup in Fig. 2. The branches of TM radiation emerged from the specimen endface with a divergence angle much less than the divergence angle of the TE radiation. This observation is consistent with a larger beam aperture for the TM radiation. The beam aperture for the TM radiation is determined by the phase-matching angle and the substrate thickness whereas the aperture for the TE radiation is determined by the TE mode profile. The TM radiation forms lines of intensity on the screen which are analogous to the m-lines created by prism out-coupling. Distinct TM radiation lines are observed on the screen for each waveguide mode, since each mode propagates with a different effective index and yields a different radiation angle ϕ'. Another noticeable feature of the TM radiation is a slight curvature of the radiation line.

The radiation pattern from specimen 41 is shown in Fig. 5. This intensity pattern was recorded by imaging the viewing screen in Fig. 2 onto a ccd camera. A polarizer determines that the two horizontal strips of light positioned above

and below the centrally located bright spot are TM-polarized, while the central bright spot is TE-polarized. The top TM radiation line corresponds to branch A while the bottom TM radiation line corresponds to branch B (refer to Fig. 3). Note in Fig. 5 the unequal power in the two branches of the TM radiation. It is possible to preferentially excite the fundamental waveguide mode or excite all the remaining higher-order waveguide modes of specimen 41. The radiation pattern shown in Fig. 5 is a result of exciting the fundamental waveguide mode.

Figures 6 and 7 provide a detailed view of the TM radiation pattern in branch A from two waveguide specimens; Figure 6 shows the TM radiation from specimen 53, while Fig. 7 shows the TM radiation pattern from specimen 41 (the titanium in-diffused waveguide). Note the intensity minimum in Fig. 6, which corresponds to the on-axis TE propagation in specimen 53. This intensity minimum is not present in of any of the modes in the titanium in-diffused specimens as illustrated in Fig. 7. Another feature in Fig. 7 is the two groups of TM radiation lines within branch A from specimen 41. These two horizontal stripes are a result of simultaneously exciting both the lowest-order mode and the higher-order modes of specimen 41. The bottom stripe in Fig. 7 corresponds to the lowest-order mode while the top stripe corresponds to higher-order modes.

The angle ϕ' at which the TM radiation line emerges from the waveguide was measured for the fundamental TE mode of specimen 41. This angle was measured by inverse triangulation. The measured value of the radiation angle is $\phi' = 34.65 \pm 0.05°$ and corresponds to a phase-matching angle $\phi = 14.39 \pm 0.02°$ within the specimen. Compare this value of ϕ to the value $\phi = 14.16 \pm 0.03°$ calculated using the measured ΔN_{eff} of Table I and Equation (4). There is a discrepancy of $0.23 \pm 0.05°$ between these two methods of calculating ϕ. Either the value of ΔN_{eff} must decrease by 0.0023 or the value of ϕ' must decrease by

0.64° in order for these values of ϕ to equal. Both of these changes lie outside the experimental errors. We cannot account for this discrepancy.

We investigate the temporal properties of the polarization coupling using two experiments. The first experiment determines whether there is a turn-on delay between the input of TE light and the observation of TM light. This experiment consists of translating the input fiber parallel to the plane of the waveguide while maintaining coupling to the TE modes. We observe the TM radiation pattern as the input coupling position is translated. We found that the translation of the TM radiation pattern coincides with the movement of the TE input coupling position within a time of less than 1 s. This measurement was limited by the minimum response time of the human eye.

The second experiment investigates the temporal response of the polarization coupling to amplitude-modulated TE light. This experiment consisted of chopping the input-coupled TE light from the HeNe laser while monitoring the TM radiation with a power meter. No time delay greater then 0.45 ms was observed. Time delays less than 0.45 ms could not be measured due to instrument limitations.

The polarization coupling ratio ρ was measured for specimens, 41, 42, and 53. Values of ρ are shown in Table II along with the measured values for the TE input power and the measured values of the TM power in branch A, the length of the specimen, and the value for the compensation factor. The multiple entries in Table II for specimen 41, which have the same input TE power, correspond to the situations where different groups of waveguide modes were selectively excited by adjusting the input coupling.

No change in the TM radiation was observed when we illuminate the specimens with the white-light source.

When the input fiber source was oriented so that TM polarization was cou-

pled into the waveguides, no TE radiation modes were observed for any of the waveguide specimens.

V. DISCUSSION

Our experimental results explicitly demonstrate the coupling between TE-polarized guided modes that propagate along the substrate's x-axis and TM-polarized radiation modes in Ti:$LiNbO_3$ slab waveguides. Summarizing the observed characteristics of this polarization coupling, we found that the power in the TM radiation is linear with the TE input power, the TM onset time is < 0.45 ms, which is less than the $10 - 1000$ s onset time found in photorefractive processes [2,24], the TM radiation angle corresponds closely to the phase matching condition to the TE guided mode, polarization coupling occurs for the fundamental and higher order TE modes, and the coupling ratio decreases with increasing diffusion time.

We do not observe this polarization coupling in $LiNbO_3$ slab waveguides formed without titanium in-diffusion but otherwise fabricated using similar procedures. Thus, we conclude that this on-axis polarization coupling is directly or indirectly attributed to titanium in-diffusion. The remainder of this section discusses a mechanism from which this on-axis polarization coupling could originate.

A. Polarization coupling through rotation of the principal dielectric axes

A mechanism certain to cause TE and TM polarization coupling would be the rotation of the waveguide region's principal axes relative to the substrate reference axes. In general, these hybrid modes contain all polarization components and, in certain cases, have characteristics similar to the mode coupling we observe.

Rotations of the principal axes can come about from the presence of particular lattice strains through the photo-elastic properties of lithium niobate. Strains, in the form of lattice contractions, have been verified and measured in titanium in-diffused lithium niobate [25–27]. In fact, these strains, in combination with the photo-elastic effect might contribute to the increase in refractive index observed in titanium in-diffused lithium niobate [25,28]. We consider the possibility that these lattice strains rotate the principal dielectric axes through the photo-elastic effect in the titanium in-diffused region.

The photo-elastic effect has also been called upon to explain hybrid mode propagation in proton-exchanged lithium niobate slab waveguides [27]. Later, this mechanism was again used to explain hybrid mode propagation in high temperature proton-exchanged lithium niobate slab waveguides [29].

The optical properties of lithium niobate are described by the relative dielectric tensor $\underline{\underline{\epsilon}}$. The relative dielectric tensor for lithium niobate in the substrate's principal axis coordinate system is

$$\underline{\underline{\epsilon}} = \begin{pmatrix} \epsilon_x & 0 & 0 \\ 0 & \epsilon_y & 0 \\ 0 & 0 & \epsilon_z \end{pmatrix}, \tag{6}$$

where the ordinary refractive index is

$$n_o \equiv \sqrt{\epsilon_x} = \sqrt{\epsilon_y} \tag{7}$$

and the extraordinary refractive index is

$$n_e \equiv \sqrt{\epsilon_z}. \tag{8}$$

Equation (6) is the form of the relative dielectric tensor used to solve for slab waveguide modes when the mode propagation directions and the crystal's principle axes coincide. Solutions to the wave equation for this case describe true TE-

and TM-polarized modes. For the general case of off-axis mode propagation, or equivalently rotation of the principal dielectric axes, coupling between all six field components takes place. We designate the rotated dielectric tensor as $\underline{\underline{\epsilon}}'$. The fields are coupled through the nonzero off-diagonal elements in $\underline{\underline{\epsilon}}'$. The presence of these off-diagonal elements can be the result of a particular strain field acting through the photo-elastic effect. We will discuss the effects of strains on mode propagation in a slab waveguide and compare theoretical predictions to our experimental results. First, we offer a brief introduction to the nomenclature describing the photo-elastic effect.

Changes to the dielectric tensor $\underline{\underline{\epsilon}}$ caused by the photo-elastic effect are described through changes to the impermeability tensor $\underline{\underline{\eta}}$. The impermeability tensor is defined to be the inverse of the dielectric tensor

$$\underline{\underline{\eta}} \equiv \underline{\underline{\epsilon}}^{-1}. \tag{9}$$

The change in the ith element of the impermeability tensor due to the photo-elastic effect is [30,31]

$$\Delta\eta_i = \sum_{j=1}^{6} p_{ij} S_j;\ i,j = 1,\ldots,6, \tag{10}$$

where the p_{ij} is an element of the elasto-optic tensor and S_j is an element of the strain tensor. We are using contracted indices $(i,j = 1,\ldots,6)$ to identify tensor elements. Each numeral subscript represents a pair of axes in the substrate coordinate system according to: $1 = xx$, $2 = yy$, $3 = zz$, $4 = yz = zy$, $5 = xz = zx$, and $6 = xy = yx$.

The new impermeability tensor $\underline{\underline{\eta}}'$ showing the modifications due to the photo-elastic effect is

$$\underline{\underline{\eta}}' = \underline{\underline{\eta}} + \Delta\underline{\underline{\eta}}. \tag{11}$$

The new dielectric tensor $\underline{\underline{\epsilon}}'$ is found by taking the inverse of $\underline{\underline{\eta}}'$ according to Equation (9).

Now we examine the specific photo-elastic induced modifications to $\underline{\underline{\epsilon}}$ using the elasto-optic tensor for lithium niobate and the lattice strain fields due to titanium in-diffusion. The contracted form of the fourth-rank elasto-optic tensor for bulk lithium niobate showing the eight independent elements is [32]

$$\underline{\underline{\underline{\underline{p}}}} = \begin{pmatrix} p_{11} & p_{12} & p_{13} & p_{14} & 0 & 0 \\ p_{12} & p_{11} & p_{13} & -p_{14} & 0 & 0 \\ p_{31} & p_{31} & p_{33} & 0 & 0 & 0 \\ p_{41} & -p_{41} & 0 & p_{44} & 0 & 0 \\ 0 & 0 & 0 & 0 & p_{44} & p_{41} \\ 0 & 0 & 0 & 0 & p_{14} & \frac{1}{2}(p_{11} - p_{12}) \end{pmatrix} \tag{12}$$

where the value of the elements is given in [33]. We assume that using the bulk elasto-optic tensor is appropriate for our discussion of the photo-elastic effect within the titanium in-diffused region. Furthermore, the values for p_{ij} we use represent the total effect of a strain field on the optical properties of lithium niobate. As discussed in [32], the total effect includes the primary modification due to the photo-elastic effect and a secondary modification due the combination of the piezoelectric and electro-optic effects.

Next, we must determine the elements of strain tensor $\underline{\underline{S}}$ which describe the strain field present in the titanium in-diffused region. We will have to consider only strains along the principal axes of the crystal since we are dealing with a static strain field. The strain along the crystal's x-axis is S_1, the strain along the crystal's y-axis is S_2, and the strain along the crystal's z-axis is S_3. Thus, in our case, the general form of the strain tensor has nonzero elements only along the diagonal

$$\underline{\underline{S}} = \begin{pmatrix} S_1 \\ S_2 \\ S_3 \\ 0 \\ 0 \\ 0 \end{pmatrix}. \tag{13}$$

Using Equations (9) through (13), we find the only nonzero off-diagonal element of the rotated dielectric tensor $\underline{\underline{\epsilon}}'$ is ϵ_4'. This element depends on the strain field according to

$$\epsilon_4' \propto \epsilon_2 \, \epsilon_3 \, p_{41} \, (S_2 - S_1), \tag{14}$$

where we take

$$p_{41} = 0.154 \tag{15}$$

as in [33]. The proportionality factor in Equation (14) is a function of all three strain elements, ϵ_2, ϵ_3, p_{12}, p_{31}, p_{41}, p_{11}, p_{13}, and p_{33}. From Equation (14) we notice the following condition on ϵ_4':

$$\epsilon_4' = 0 \text{ if } S_1 = S_2 \text{ or if } S_1 = S_2 = 0. \tag{16}$$

Next, we discuss the specific strains present in the titanium in-diffused region. Several groups have measured the lattice strain in the titanium in-diffused region on y-cut lithium niobate. A lattice contraction is found in each case. However, there is disagreement regarding the nonzero terms of $\underline{\underline{S}}$. We present three examples from the literature which use different strain elements in their analysis of slab waveguides formed by titanium in-diffusion on y-cut lithium niobate. In the first example a nonzero strain S_2 was measured in y-cut slab waveguides [25]. The

strain S_1 was assumed to be equal to S_2 and the strain S_3 was calculated using S_2. In contrast, the authors of [28] use symmetry arguments to determine the only nonzero strain element would be S_2 in y-cut slab waveguides. In comparison, the third example [27] reports that $S_2 = 0$ while both S_1 and S_3 are nonzero.

According to Equation (16), there will not be any off-diagonal elements in $\underline{\underline{\epsilon}}'$ if $S_1 = S_2$. Thus, the strain field described in the first example would not couple TE- and TM-polarized modes. However, in the second and third examples there would be off-diagonal terms in $\underline{\underline{\epsilon}}'$ corresponding to crystal axis rotation; consequently there would be coupling of the TE and TM polarized modes.

We cannot accurately model the crystal axis rotation caused by the photo-elastic effect without a consensus regarding the strain elements present in the diffused region. However, since we think that the photo-elastic effect is causing the polarization coupling, we will proceed by assuming the only nonzero element of strain is S_2. We base our assumption on the opinion that the substrate anchors the lattice dimensions that are parallel to the plane of the waveguide. Thus, S_1 and S_3 are 0 due to the influence of the unperturbed substrate lattice spacing. Contrarily, the lattice spacing perpendicular to the plane of the waveguide is free to experience strains resulting from titanium in-diffusion. Next, we calculate the effects on the dielectric tensor from the strain S_2.

We need to know the relationship between titanium concentration and strain in order to calculate the strain S_2 in the in-diffused region. We found this relationship from the data presented in [25]. We use measurements of strain S_2 and surface titanium concentration from a y-cut, titanium in-diffused lithium niobate specimen that was in-diffused for 10 h at 1000 °C . We find the relationship between strain S_2 and titanium concentration $C_s(\mathrm{Ti})$ is

$$S_2 = -9.5 \times 10^{-25} C_s(\mathrm{Ti}) \tag{17}$$

where the units of titanium concentration are atoms/cm ^{3}. We assume the linear relationship of Equation (17) holds over the range of titanium concentrations found in our specimens. We find different values for the proportionality constant in Equation (17) using the data in [25] for specimens fabricated similarly except with different diffusion temperatures. Values of $S_2/C_s(\mathrm{Ti})$ are plotted against diffusion temperature in Figure 8. We speculate that this variation in $S_2/C_s(\mathrm{Ti})$ is a result of the titanium ions residing at different lattice sites corresponding to different diffusion temperatures.

The strain within the titanium in-diffused region of waveguide specimen 42 is calculated using Equation (17), and the measured titanium concentration is plotted in Figure 4. The resulting strain profile is plotted in Figure 4. The maximum contractive strain occurs at the surface and has a value of -2.2×10^{-3}. The magnitude of this maximum contractive strain is greater than the breaking strain (2×10^{-4}) resulting from thermal expansion in lithium niobate reported in [34]. In fact, the magnitude of the strain in specimen 42 is greater than the breaking strain until a depth greater than 2.2 μm.

These calculations show that the titanium in-diffused region will consist of different layers each with its principal dielectric axes oriented differently because of the nonuniform strain field. We calculate the rotated dielectric tensor $\underline{\underline{\epsilon}}'$ at several depths within the titanium in-diffused region using the strain profile of Figure 4. Then, we reduce $\underline{\underline{\epsilon}}'$ to its diagonal form to find values of the new principal refractive indices (n'_x, n'_x and n'_x) corresponding to new principal dielectric axes (x', y', z'). The rotation angles $\alpha_{x,y,z}$ are defined as the angles between the substrate principal dielectric axes (x, y, and z in Figure 1) and the corresponding

new principal dielectric axes of $\underline{\underline{\epsilon}}'$. We also calculate the difference between the new and the old principal refractive indices $\Delta n_{x,y,z} = n'_{x,y,z} - n_{x,y,z}$. The rotation angles and the principal refractive index differences are plotted in Figure 9. The new principal axes experience a rotation about the mode propagation axis (x-axis). The maximum rotation angle is $\alpha_y = \alpha_z = 1.3°$. Also, the refractive indices n_x and n_y change by different amounts. Thus, the titanium in-diffused region becomes biaxial.

For comparison, a crystal axis rotation of less than 1° was calculated in [27] for proton-exchanged lithium niobate waveguides. In another study [29], a crystal axis rotation of 10° about the x-axis was used to fit theoretical calculations to measured values of hybrid mode effective indices in proton exchanged slab waveguides in x-cut lithium niobate.

The waveguide geometry resulting from this depth-dependent rotation of the principal dielectric axes is complex. Traditionally, the titanium in-diffused region is modeled as a region characterized as graded-index, uniaxial anisotropic and uniformly oriented principal axes. However, in the presence of photo-elasticity, the titanium in-diffused region has a depth dependent biaxial anisotropy and a depth dependent principal axes orientation.

We know this waveguide geometry will couple the z-directed electric field (TE) with the y-directed electric field (TM). We also know the y-directed field is not guided and will radiate from the waveguide region. This is so because the phase-matching condition between the TE and TM fields does not simultaneously satisfy the TM waveguide condition. We cannot be more specific about waveguide mode characteristics without solving the electro-magnetic boundary value problem for this geometry.

We are not aware of any investigations analyzing a waveguide geometry of

the same complexity as our waveguide geometry. There have been investigations into the modal properties of waveguides formed from 3 step-index layers, each with own arbitrary anisotropic properties [7]. A multi-layer approach was used in [12] to analyze graded-index waveguides of uniaxial anisotropy. Certainly, an approach combining these two methods would provide the capabilities to analyze the waveguide geometry of interest here.

VI. SUMMARY

We have observed polarization coupling form TE guided modes to TM radiation modes in titanium in-diffused lithium niobate slab waveguides. The characteristics of this polarization coupling are not the same as the polarization coupling that originates from photo-refractive effects. We hypothesize the polarization coupling we observe is the result of the photo-elastic effect. The photo-elastic effect transforms the titanium in-diffused waveguide region into one with a complex geometry. Still, this waveguide geometry is amenable to analysis by numerical techniques.

VII. ACKNOWLEDGMENTS

We acknowledge the support of the National Science Foundation under grant number ECS-9015752, the United States Army Research Office under grant number DAAL-03-92-G-0289 and the Office of Naval Research under grant number DOD ONR 14-92-J-1190. We also acknowledge many helpful editorial comments from Dr. Matt Young.

REFERENCES

[1] R. V. Schmidt and I. P. Kaminow, "Metal-diffused optical waveguides in $LiNbO_3$ films," *Appl. Phys. Lett.*, vol. 25, pp. 458–460, 1974.

[2] P. G. Kazansky, "Photo-induced conversion of radiation polarization in integrated optics components based on $LiNbO_3$," *IEEE J. Quantum Electron.*, vol. 25, pp. 736–741, 1989.

[3] R. Chen and W. S. C. Chang, "Anomalous attenuation and depolarization scattering in y-cut $LiNbO_3$ proton exchanged waveguides," *IEEE J. Quantum Electron.*, vol. 22, pp. 880–881, 1986.

[4] D. P. Russo and J. H. Harris, "Wave propagation in anisotropic thin-film optical waveguides," *J. Opt. Soc. Amer.*, vol. 63, pp. 138–145, 1973.

[5] M. O. Vassell, "Structure of optical guided modes in planar multilayers of optically anisotropic materials," *J. Opt. Soc. Amer.*, vol. 64, pp. 166–173, 1974.

[6] W. K. Burns and J. Warner, "Mode dispersion in uniaxial optical waveguides," *J. Opt. Soc. Amer.*, vol. 64, pp. 441–446, 1974.

[7] M. S. Kharusi, "Uniaxial and biaxial anisotropy in thin-film optical waveguides," *J. Opt. Soc. Amer.*, vol. 64, pp. 27–35, 1974.

[8] D. Marcuse, "Modes of a symmetric slab optical waveguide in birefringent media-part 1: Optical axis not in plane of slab," *IEEE J. Quantum Electron.*, vol. 14, pp. 736–741, 1978.

[9] D. Marcuse, "Modes of a symmetric slab optical waveguide in birefringent media-part 2: Slab with coplanar optical axis," *IEEE J. Quantum Electron.*,

vol. 15, pp. 92–101, 1979.

[10] P. Yeh, "Electromagnetic propagation in birefringent layered media," *J. Opt. Soc. Am.*, vol. 69, pp. 742–756, 1979.

[11] L. Torner, F. Canal, and J. Hernandez-Marco, "Leaky modes in multilayer uniaxial optical waveguides," *Appl. Opt.*, vol. 29, pp. 2805–2814, 1990.

[12] K. Yamanouchi, T. Kamiya, and K. Shibayama, "New leaky surface waves in anisotropic metal-diffused optical waveguides," *IEEE Trans. Microwave Theory Tech.*, vol. 26, pp. 289–304, 1978.

[13] S. K. Sheem, W. K. Burns, and A. F. Milton, "Leaky-mode propagation in Ti-diffused $LiNbO_3$ and $LiTaO_3$ waveguides," *Optics Letters*, vol. 3, pp. 76–78, 1978.

[14] Optical grade lithium niobate wafers were purchased from Crystal Technologies Inc., Palo Alto, California.

[15] I. P. Kaminow and J. R. Carruthers, "Optical waveguiding layers in $LiNbO_3$ and $LiTaO_3$," *Appl. Phys. Lett.*, vol. 22, pp. 326–328, 1973.

[16] J. R. Carruthers, I. P. Kaminow, and L. W. Stulz, "Diffusion kinetics and optical waveguiding properties of out-diffused layers in lithium niobate and lithium tantalate," *Appl. Opt.*, vol. 13, pp. 2333–2342, 1974.

[17] S. L. Kwiatkowski and A. R. Mickelson, "Nearly cut-off modes caused by diffusion in lithium niobate," *J. Appl. Phys*, 1994. scheduled to appear in the 1 November.

[18] P. K. Tien, "Light waves in thin films and integrated optics," *Appl. Opt.*, vol. 10, pp. 2395–2413, 1971.

[19] T. Tamir, *Integrated Optics.* Berlin, New York: Springer-Verlag, second ed., 1985.

[20] W. L. Bond, "Measurement of the refractive indices of several crystals," *J. Appl. Phys.*, vol. 36, pp. 1674–1677, 1965.

[21] A. Yariv, *Quantum Electronics.* New York: Wiley, second ed., 1975.

[22] SIMS measurements were performed by Steve Novak of Evans East, Plainsboro, New Jersey, USA.

[23] J. Crank, *The Mathematics of Diffusion.* New York: Oxford University Press, second ed., 1986.

[24] D. Kip, R. Fink, T. Barttholomäus, and E. Krätzig, "Coupling of orthogonally polarized waves in $LiNbO_3$ optical waveguides," *Opt. Comm.*, vol. 95, pp. 33–38, 1993.

[25] K. Sugii and M. F. ahd H. Iwasaki, "A study on titanium diffusion into $LiNbO_3$ waveguides by electron probe analysis and X-ray diffraction methods," *J. Mater. Science*, vol. 13, pp. 523–533, 1978.

[26] M. N. Armenise, M. D. Sario, C. Canali, P. Franzosi, J. Singh, R. H. Hutchins, and R. M. D. L. Rue, "In-plane scattering in titanium-diffused $LiNbO_3$ optical waveguides," *Appl. Phys. Lett.*, vol. 45, pp. 326–328, 1984.

[27] V. A. Ganshin and Y. N. Korkishko, "Deformations, stress and birefringence in proton-exchanged lithium niobate waveguides," *J. Opt. Commun.*, vol. 13, pp. 2–7, 1992.

[28] S. Fries, P. Hertel, and H. P. Menzler, "Extraordinary versus ordinary refractive index change in planar $LiNbO_3$:Ti waveguides," *Phys. Stat. Sol. (a)*,

vol. 108, pp. 449–455, 1988.

[29] S. Chen, P. Baldi, M. P. D. Micheli, D. B. Ostrowsky, A. Leycuras, G. Tartarini, and P. Bassi, "Hybrid modes in proton exchanged waveguides realized in $LiNbO_3$, and their dependence on fabrication parameters," *Opt. Lett.*, vol. 18, pp. 1314–1316, 1993.

[30] T. S. Narasimhamurty, *Photoelastic and Electro-optic properties of crystals.* New York: Plenum Press, first ed., 1981.

[31] A.Yariv and P. Yeh, *Optical Waves in Crystals.* New York: Wiley, first ed., 1984.

[32] R. S. Weis and T. K. Gaylord, "Lithium niobate: Summary of physical properties and crystal structure," *Appl. Phys. A*, vol. 37, pp. 191–203, 1985.

[33] R. J. O'Brien, G. J. Rosasco, and A. Weber, "Brillouin scattering in lithium niobate," *J. Opt. Soc. Am.*, vol. 60, p. 716, 1970.

[34] J. C. Brice, "The cracking of czochralski-grown crystals," *J. Cryst. Growth*, vol. 42, pp. 427–430, 1977.

[35] D. F. Nelson and R. M. Mikulyak, "Refractive indices of congruently melting lithium niobate," *J. Appl. Phys.*, vol. 45, pp. 3688–3689, 1974.

List of Tables

List of Figures

TABLES

TABLE I. The difference between the TE mode effective index and the substrate extraordinary index ($n_e = 2.2028$) are tabulated for the $LiNbO_3$ slab waveguides. Effective index measurements were made using prism out-coupling. Also listed are the phase-matching angles ϕ calculated using equation (4) and the substrate ordinary index $n_o = 2.2865$. The effective mode index N_{eff} was found by adding the substrate extraordinary index $n_e = 2.2028$ to the value of ΔN_{eff}. The values for n_e and n_o are from [35].

	Specimen					
	41		42		53	
Mode #	ΔN_{eff}	ϕ [°]	ΔN_{eff}	ϕ [°]	ΔN_{eff}	ϕ [°]
1	0.0142 ±0.0003	14.16	0.0127 ±0.0002	14.32	0.0025 ±0.0004	15.32
2	0.0028 ±0.0002	15.29	0.0046 ±0.0002	15.11	0.0015 ±0.0004	15.41
3	0.0006 ±0.0002	15.49	0.0030 ±0.0003	15.27	0.0004 ±0.0004	15.51
4			0.0014 ±0.0002	15.42		
5			0.0011 ±0.0002	15.45		

TABLE II. Measured TE-TM coupling characteristics for the $LiNbO_3$ slab waveguides.

Specimen	Conversion Ratio ρ [%-cm^{-1}]	TE Input Power [μW]	Branch A TM Power [μW]	Length L [cm]	Compensation Factor Γ	Comments
41	3.2%	83	2.1	1.9	2.4	Fundamental waveguide mode
41	3.2%	47	1.2	1.9	2.4	Fundamental waveguide mode
41	1.2%	83	0.79	1.9	2.4	Higher-order waveguide modes
41	1.2%	47	0.46	1.9	2.4	Higher-order waveguide modes
42	0.8%	63	0.68	2.8	2.2	Optimum Input fiber position for maximum TM Power
42	0.7%	62	0.56	2.8	2.2	Same as above
42	0.8%	55	0.59	2.8	2.2	Same as above
42	0.7%	40	0.37	2.8	2.2	Same as above
42	0.7%	22	0.20	2.8	2.2	Same as above
42	0.8%	11	0.11	2.8	2.2	Same as above
53	0.07%	63	0.025	1.3	2.2	Same as above

FIGURES

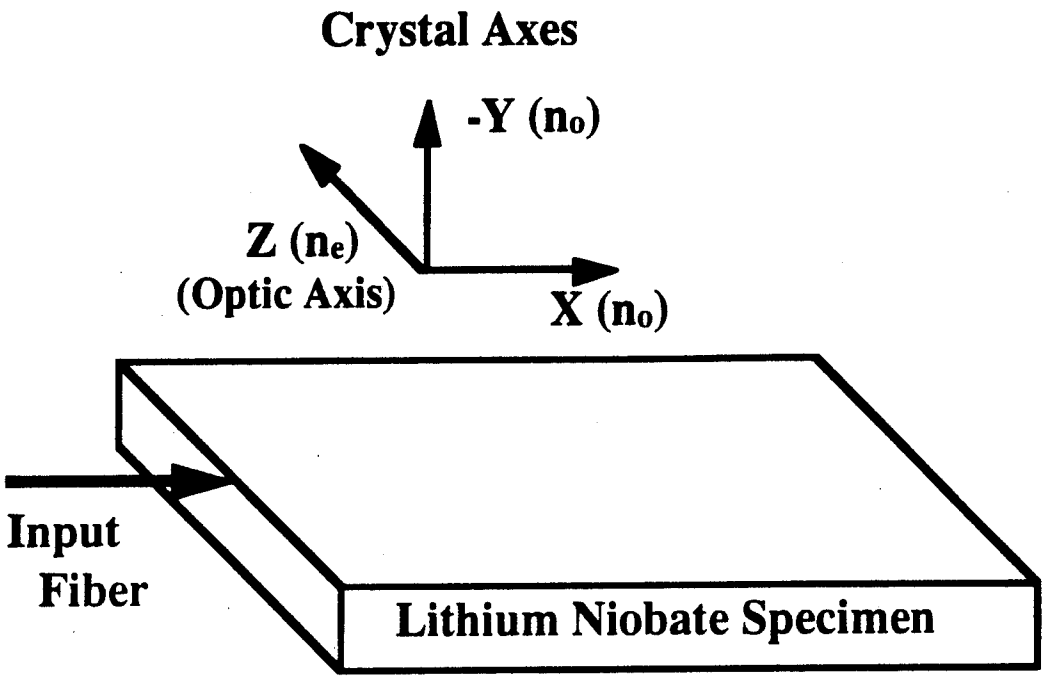

FIG. 1. The waveguide orientation and mode propagation direction relative to the $LiNbO_3$ crystal's axes. The extraordinary index is $n_e = 2.2028$ and the ordinary index is $n_o = 2.2865$ at the wavelength $\lambda = 0.6328\,\mu$m [35].

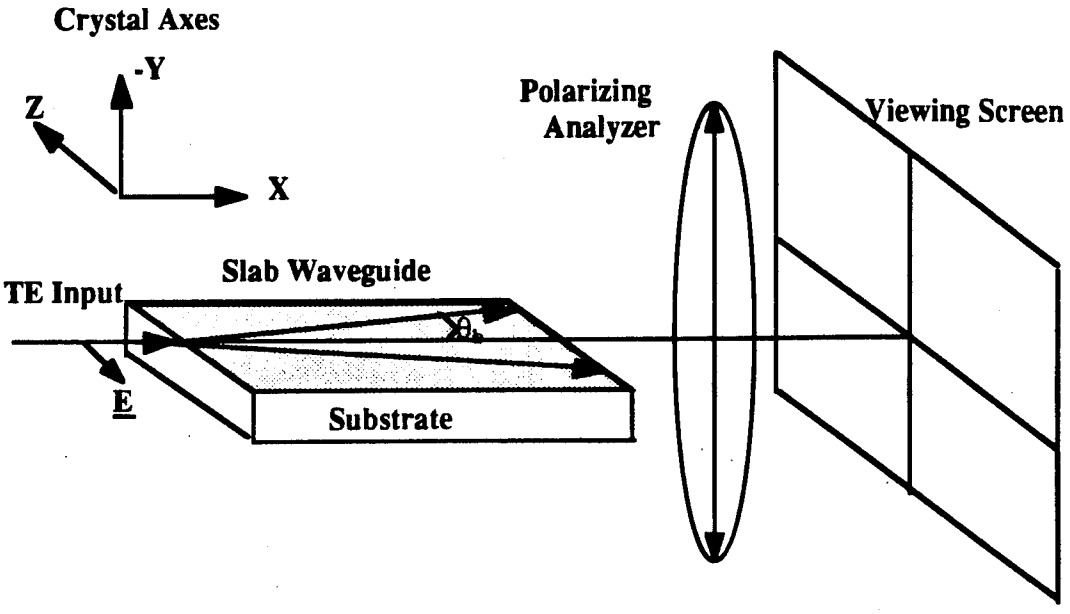

FIG. 2. The experimental setup used to observe the intensity patterns emerging from the waveguide specimens. The polarization of the emerging radiation is determined using the polarizing analyzer.

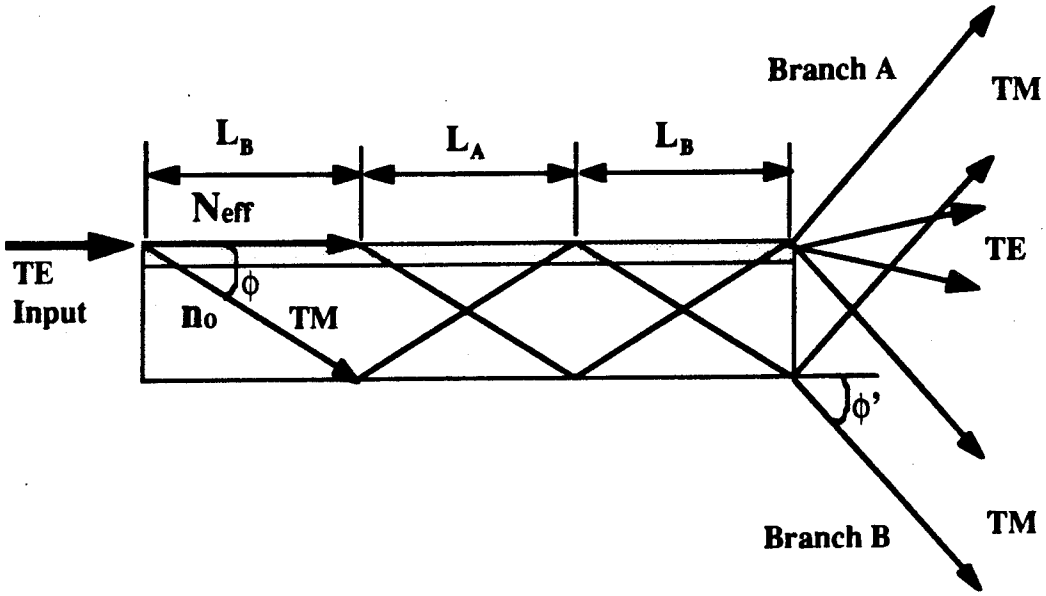

FIG. 3. Illustration of phase matching between the TE polarized waveguide and the TM radiation mode. The TE mode propagates with effective index N_{eff} while the TM mode propagates with refractive index n_o.

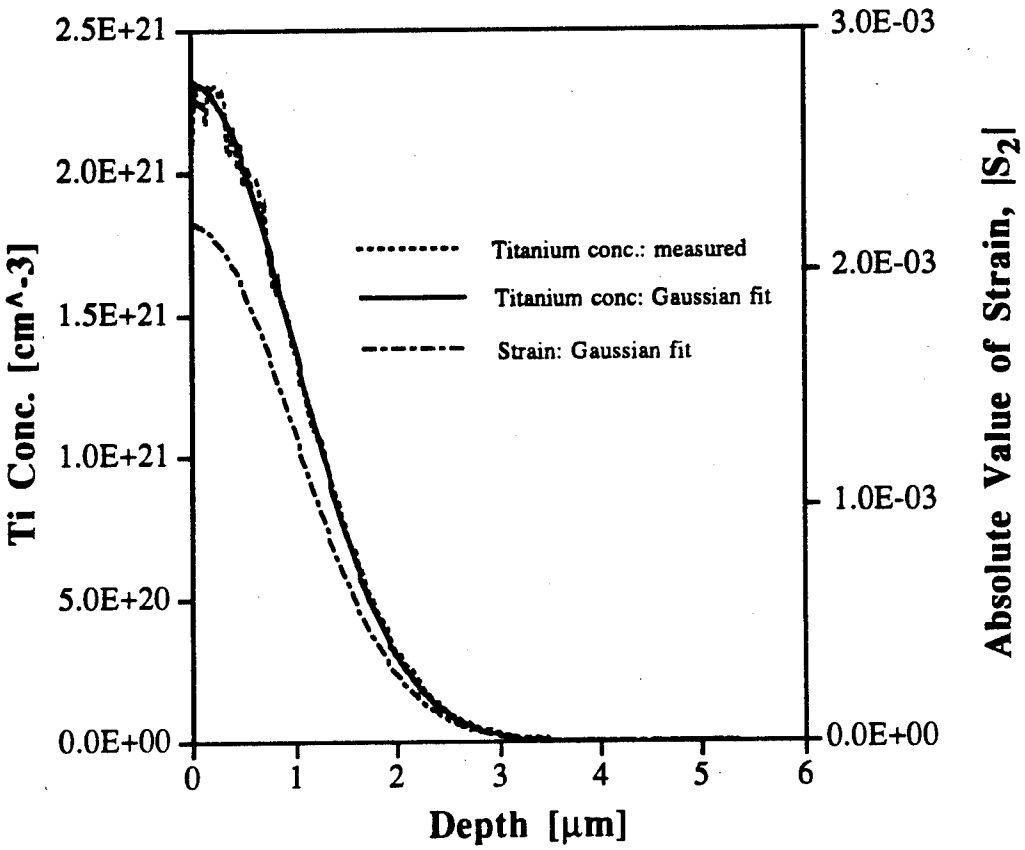

FIG. 4. Depth dependence of titanium concentration and absolute value of strain within specimen 42 after diffusion. Measured titanium concentration is compared to the Gaussian solution to the diffusion equation. The Gaussian profile was fitted with the following parameter values: the surface concentration $C_{Ti}(0)$ is 2.31×10^{21}atoms/cm^3 and the 1/e diffusion depth is 1.4 μm. The strain along the crystal's y-axis S_y is calculated using the Gaussian titanium concentration profile and the linear relationship between strain and titanium concentration calculated from the data in [25].

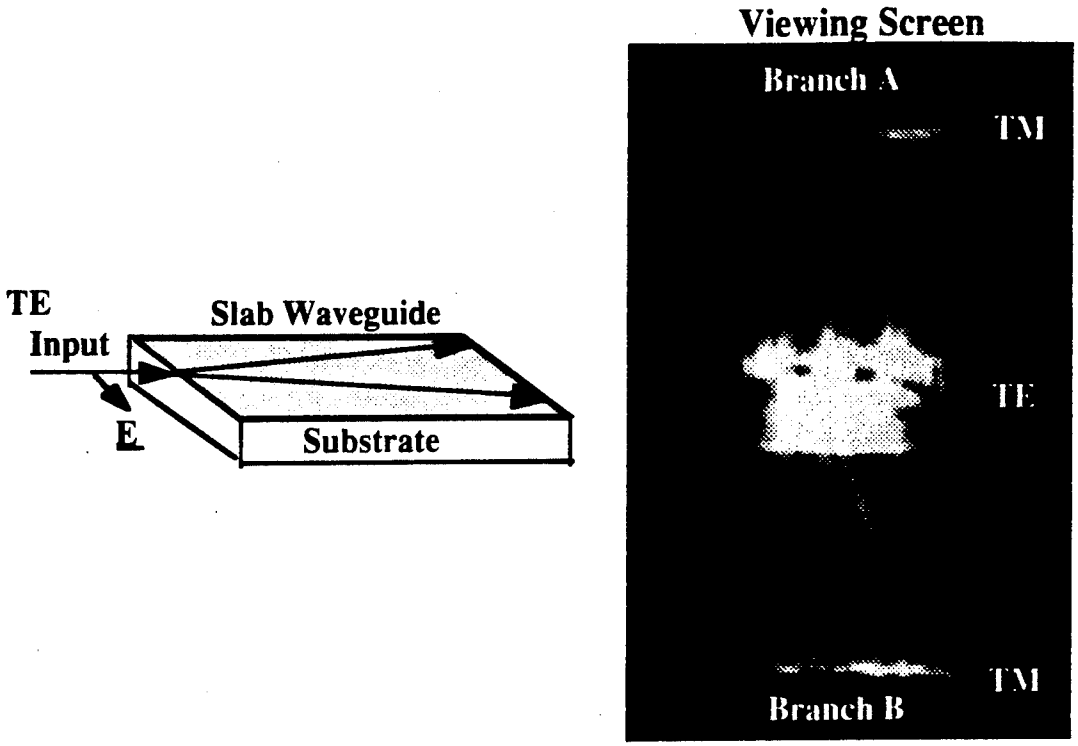

FIG. 5. Intensity pattern emerging from specimen 41 as seen on the viewing screen. The central region is TE polarized while both the upper and lower regions are TM polarized.

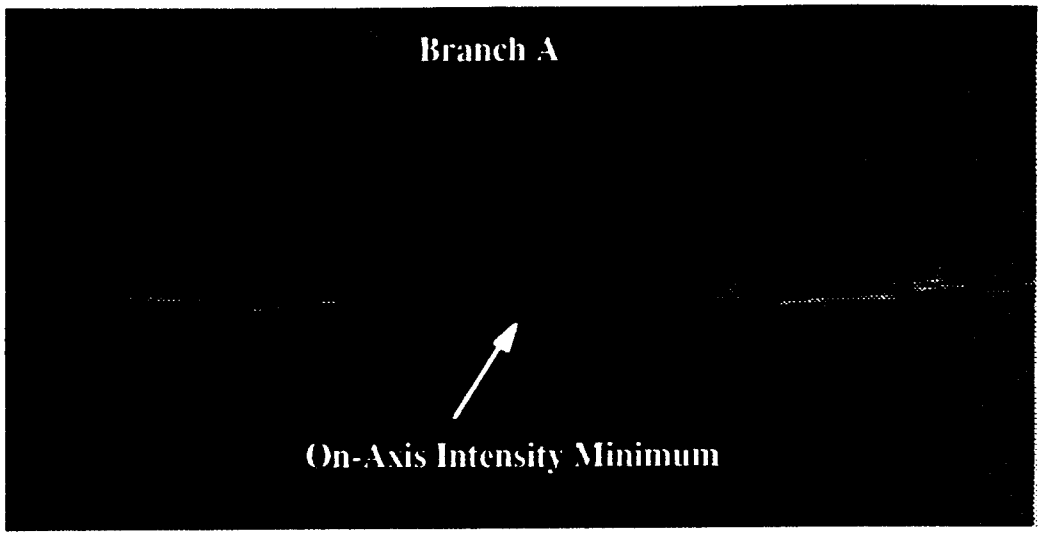

FIG. 6. Detailed view of branch A radiation from specimen 53. The on-axis intensity minimum is indicated by the arrow.

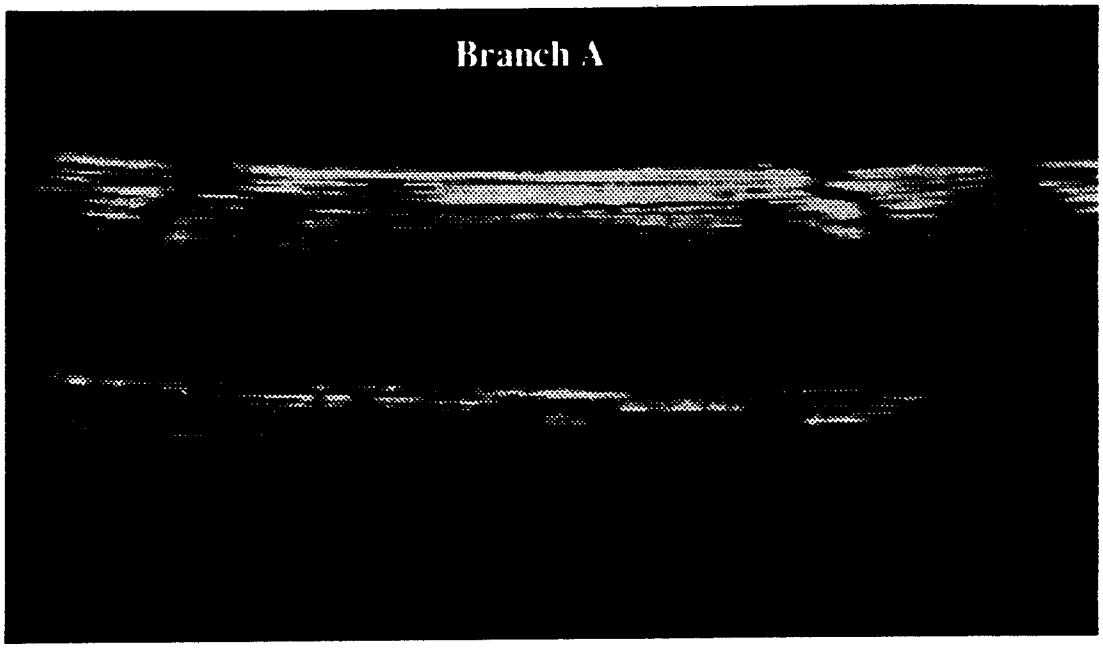

FIG. 7. Detailed view of branch A radiation from specimen 41.

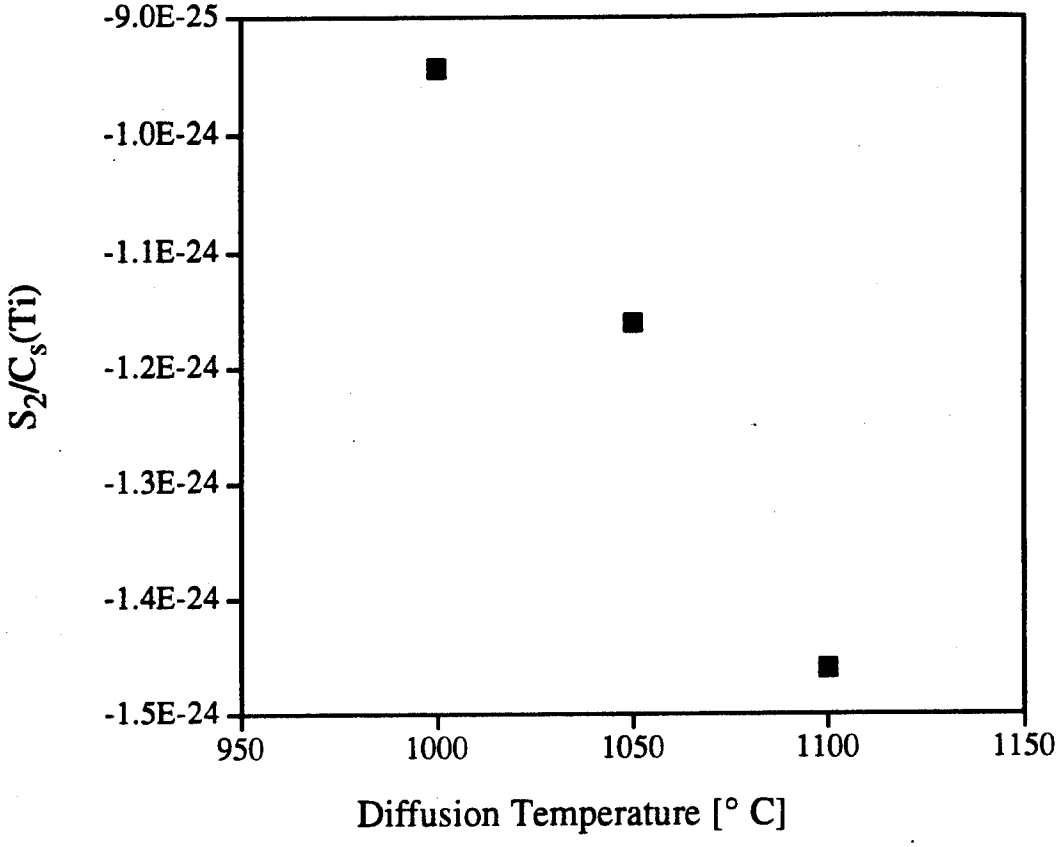

FIG. 8. Temperature dependence of $S_2/C_s(Ti)$ from [25] where S_2 is the strain along the y-axis and $C_s(Ti)$ is the surface concentration of titanium in atoms/cm^3.

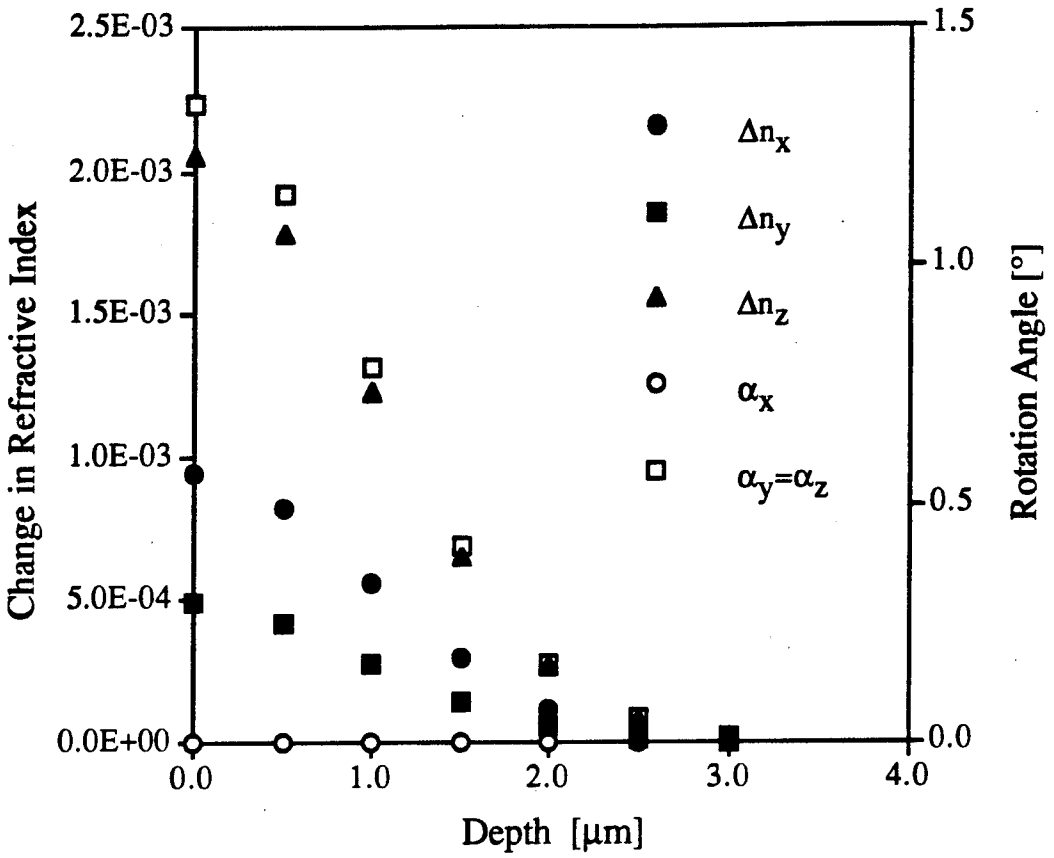

FIG. 9. Depth dependence of the change in principal refractive index Δn and the principal axes rotation angles α within specimen 42 after diffusion. The change in refractive index between the principal axes x and x' is Δn_x, between principal axes y and y' is Δn_y and between principal axes z and z' is Δn_z. The rotation angles are found by taking the vector dot product between corresponding principal dielectric axes. The angle between x and x' is α_x, the angle between y and y' is α_y and the angle between z and z' is α_z.